ELSEVIER

Heliyon

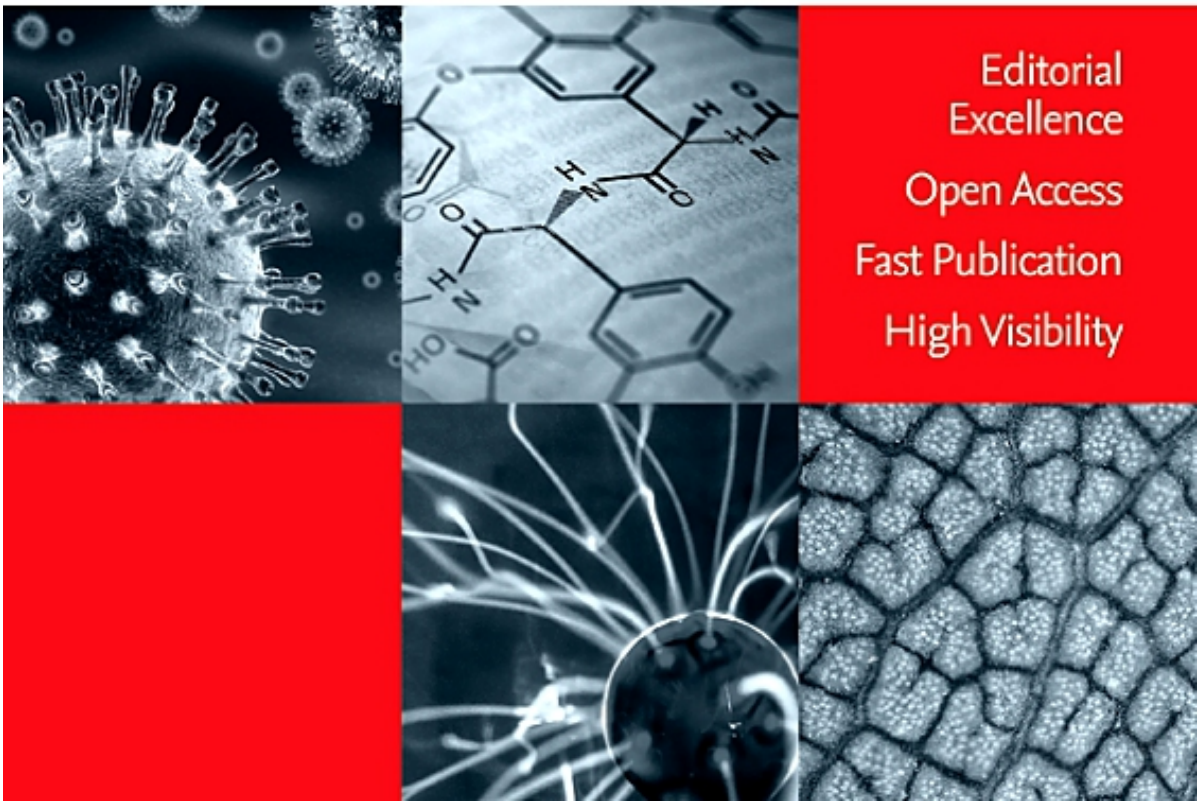

Volume 5, Issue 1, January 2019, e01114
open access

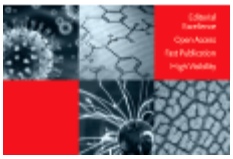

Dynamic behavior of double and triple adjacent 2D hills using boundary element method

Author links open overlay panelMobinAfzalirad[a]
MehranNaghizadehrokni[b]ImanKhosravi[c]
https://doi.org/10.1016/j.heliyon.2018.e01114Get rights and content
Under a Creative Commons license

Heliyon

Received:
3 August 2018
Revised:
17 October 2018
Accepted:
28 December 2018

Cite as: Mobin Afzalirad, Mehran Naghizadehrokni, Iman Khosravi. Dynamic behavior of double and triple adjacent 2D hills using boundary element method. Heliyon 5 (2019) e01114. doi: 10.1016/j.heliyon.2018.e01114

Dynamic behavior of double and triple adjacent 2D hills using boundary element method

Mobin Afzalirad [a,*], **Mehran Naghizadehrokni** [b], **Iman Khosravi** [c]

[a] *Civil Engineering Department, Islamic Azad University, Iran*

[b] *Chair of Geotechnical Engineering, RWTH Aachen University, Germany*

[c] *Islamic Azad University, Iran*

[*] Corresponding author.

E-mail address: m.afzali@qaemiau.ac.ir (M. Afzalirad).

Abstract

A 2D boundary element method with material damping is developed in order to seismic investigation of constructions with different configurations. The boundary element algorithm, which utilized the time-convoluted kernels is employed in order to incorporate proportional damping. In order to investigate the seismic reaction of two dimensional double and triple semi-sine formed hills subjected to vertical P and SV waves by using a developed viscoelastic boundary element algorithm and responses are presented in the form of graphs, amplification pictures and displacement. In addition, the influences of various damping proportions on site of semi-sine hills with various shapes are analyzed. It can be concluded from the results that the crest of homogeneous adjacent hills have similar shape ratio, potential and larger maximum amplification in comparison with the crest of single hills. Although this difference is increased by increasing shape ratio, it is negligible within the proportions of study shape. In addition, multiplicity of hills increased frequency characteristic of amplification curve and the number of peaks and valleys.

Keywords: Civil engineering, Mechanical engineering, Structural engineering, Geophysics

https://doi.org/10.1016/j.heliyon.2018.e01114
2405-8440/© 2018 Published by Elsevier Ltd. This is an open access article under the CC BY-NC-ND license (http://creativecommons.org/licenses/by-nc-nd/4.0/).

1. Introduction

The effect of local conditions of geology and soil have been investigated on the severity of ground vibration and earthquake damage in recent years. Earth seismic behavior is affected by different parameters: influence of source, propagation direction influence and site influence [1, 2, 3]. One of the well-known site effects is the topography of the earth's surface since the incoming waves field can be modified by this surface topographical irregularity [4]. Previous numerical studies on seismic behavior of topographic features were mainly limited to their single form. Whereas, a realistic look at the surrounding nature shows the high diversity and complexity of the ground surface and topographic features often appear in complex form. Among a number of numerical studies conducted on the seismic behavior of hills, a considerable amount of studies is devoted to single semi-sine hills. The reason is that the semi-sine hills are the most common form of natural topography of ground surface. These studies showed that the hills can influence different points of the ground's surface with amplification of the motion component amplitude as well as the phase difference between adjacent points of the seismic response.

Observations by Trifunac, Hudson and Boore in San Fernando earthquake 1971 in Pacoima dam that showed a maximum horizontal acceleration about 1.25g in the two perpendicular directions which was recorded by seismograph located on the crest of a rocky hill [5, 6, 7, 8] and Lee et al., after the Northridge earthquake in 1994 in Tarzana hills [9, 10], were the starting point of investigation. Then various numerical and analytical studies were done to calculate the seismic behavior of natural topography of the ground's surface. Researchers found that one of the reasons for recording high accelerations in Pacoima dam site at the time of the earthquake in San Fernando 1971 [5, 6] and observations of the earthquake in Chile 1985 [11] was topographic effects.

Davis and West considered the influence of topography for analyzing site. During the experiment, which was conducted in the Nevada desert in 1968, accelerographs installed in and out of Tonopah City showed different measurements, while Tonopah was in a valley and accelerographs installed near the mountain. However, since the procedure of placing accelerographs was not suitable for providing spectrum amplification values, attempts were done to consider the effect of topography for studying site response [12].

Bard stated that there is a good agreement between seismic movements observed on the top of mountains and at the bottom of valleys, respectively, with the results of theoretical and numerical studies. He indicated that the ground vibration amplification on the top of mountains is usually more for horizontal components than the vertical ones that the horizontal component and vertical component are caused by S waves and P waves. The difference between the two horizontal components is

https://doi.org/10.1016/j.heliyon.2018.e01114
2405-8440/© 2018 Published by Elsevier Ltd. This is an open access article under the CC BY-NC-ND license (http://creativecommons.org/licenses/by-nc-nd/4.0/).

considerable. Bard showed that the maximum amplification is associated with a sharpness of topography and the amplification will increase by growing the slope of topography [13].

Kamalian et al. used time domain 2D BEM for analyzing response of 2D ridges and valleys. In addition, different basic rules presented for the seismic design of structures with various 2D topographic structures. Although, they provide the findings achieved by an extensive numerical study on seismic behavior of two dimensional semi-sine formed hills, the formulation adopted was limited to a linear elastic medium except for the effects of material damping on site response [14, 15, 16, 17, 18, 19, 20]. Later, Chaillat studied the seismic behavior of topographic features by utilizing fast baoundary element method in frequency space and for visco-elastic environments. They have accelerated the standard BEM by using fast multipole method and have developed the basic elastodynamic responses based on this method [21].

Sohrabi Bidar et al., presented elastodynamic 3D cores with analytical solutions of convolution integrals of traction basic responses in two constant and linear changes. Based on boundary element algorithm and 3D elastodynamic cores, they provided BEMSA (boundary element method for 36 seismic analyses) software, which is used for dynamic analysis of 3D topographic effects [22, 23].

Vincenzo assessed the site effect and its relationship with local topographical features of a slope. A FEM is employed to calculate the seismic amplification. In this paper, models are considered horizontally and unlimited at the slope's crest and foot. Input waves utilized in this investigation, is a SV seismic wave in different frequency 0.5−32 Hz [24]. Moreover, Cavallaro et al., examined the effect of topography on Monte Po hill where is located in an area with high seismic hazard. They analyzed the hill behavior using one and two-dimensional method, and examined the results [25].

Review of technical literature, especially the aforementioned works indicates that no comprehensive numerical studies have been done on seismic behavior of the compound hills. Most researches are restricted to single hills and in the frequency space and no studies were performed on time space. The principal object of this investigation is to discuss the findings of BEM on seismic behavior of double and triple adjacent 2D homogenous semi-sine hills with material damping.

For this purpose, the simplest combination of adjacent hills including double and triple semi-sine hills are considered. First, the seismic behavior of the double homogenous adjacent hills is examined and is compared with single hills; then the seismic behavior of triple homogenous adjacent hills as well as the behavior in the valley between two hills is considered. An attempt is made to analyze the results of numerical sensitivity study and infer the initial answers to three key questions: how and to

https://doi.org/10.1016/j.heliyon.2018.e01114
2405-8440/© 2018 Published by Elsevier Ltd. This is an open access article under the CC BY-NC-ND license (http://creativecommons.org/licenses/by-nc-nd/4.0/).

what extent can adjacency of double semi-sine adjacent hills increase the amplification potential of each of them? Can the behavior of valley between two adjacent hills be equivalent to the seismic behavior of a single valley with the same shape? Can the adjacency of hills easy interpret large amounts of amplification ratios observed in experimental studies for earlier researchers?

2. Methodology

2.1. Governing equations

The numerical research was implemented through developing a two-dimensional visco-elastodynamics. The fundamental equation for a body may be presented as Eq. (1):

$$\left(c_1^2 - c_2^2\right) \cdot u_{j,ij} + c_2^2 \cdot u_{i,jj} + b_i - \ddot{u}_i = 0 \tag{1}$$

In the above equation u_i and b_i are the movement vector the body force vector, respectively and the propagation velocities of the compression and shear waves can be introduced by c_1 and c_2, which are given by $C_1^2 = (\lambda + 2\mu)/\rho$; $C_2^2 = \mu/\rho$, with λ and μ being the Lame constants and ρ the mass density.

The fundamental boundary integral equation for the elastic, isotropic and homogeneous half-plane exposed to an incoming in-plane movement ($u_j^{inc.}$), may be achieved utilizing the weighted residual procedure as Eq. (2) [26]:

$$c_{ij}(s).u_i(s,t) = \int_{\Gamma} \left(G_{ij}^*(x,s,t)*t_i(x,t) - H_{ij}^*(x,s,t)*u_i(x,t) \right) \cdot d\Gamma + u_j^{inc.}(s,t) \tag{2}$$

In which, G_{ij} and H_{ij} can be recognized as the transient movement and traction fundamental solutions.

Integrating by parts can result in the below superseded boundary integral equation, which is as follows Eq. (3) [27]:

$$c_{ij}(s).u_i(s,t) = \int_{\Gamma} \left(G_{ij}^*(x,s,t)*p_i(x,t) - Z_{ij}^*(x,s,t)*u_i(x,t) + W_{ij}^*(x,s,t)*v_i(x,t) \right) d\Gamma + u_j^{inc.}(s,t) \tag{3}$$

In which, v_i is the velocity vector and G_{ij}^*, Z_{ij}^* and W_{ij}^* represent the corresponding solutions for movement, traction and velocity, subsequently.

Assume that a unit point force is applied at a two-dimensional body at time t=0. If the body has a liner elastic behavior, the displacement at time t is thought to be $u_\circ(t)$. In addition, if the body has viscoelastic behavior, the displacement at time t, equals

https://doi.org/10.1016/j.heliyon.2018.e01114
2405-8440/© 2018 Published by Elsevier Ltd. This is an open access article under the CC BY-NC-ND license (http://creativecommons.org/licenses/by-nc-nd/4.0/).

to Eq. (4) considering material damping. This has been carried out successfully by Feng et al., [28]:

$$u(t) = u_{\circ}(t)(1-\eta)^{\frac{(t-\tau)}{2T}} \tag{4}$$

In Eq. (4), T denotes the prominent period of earthquake loading, approximately and η denotes the coefficient of proportional damping.

According to Eq. (5), the boundary integral equation, Eq. (3) takes the following modified form for a viscoelastic body:

$$\begin{aligned} c_{ij}(s).u_j(s,t) = & \int_0^t \left[\int_\Gamma \left(G^*_{ij}(x,s,t-\tau).p_i(x,t) \right) d\Gamma \right] (1-\eta)^{(t-\tau)/2T} d\tau \\ & + \int_0^t \left[\int_\Gamma \left(W^*_{ij}(x,s,t-\tau).v_i(x,t) \right) d\Gamma \right] (1-\eta)^{(t-\tau)/2T} d\tau \\ & - \int_0^t \left[\int_\Gamma \left(Z^*_{ij}(x,s,t-\tau).u_i(x,t) \right) d\Gamma \right] (1-\eta)^{(t-\tau)/2T} d\tau + u^{inc.}_{jd}(s,t) \end{aligned} \tag{5}$$

Where $u^{inc.}_{jd}(s,t)$ is damped incident wave.

2.2. Theory

The executed of boundary integral in Eq. (3) requires estimation in both temporal and spatial changes of the field parameters. For temporal integration, the time axis from 0 to t is divided into N equal steps of duration Δt, i.e. $t = N.\ \Delta t$. Application of a linear time variation of the field variables, the displacement, velocity and traction are represented as follows in Eqs. (6), (7), and (8):

$$u_i(x,\tau) = \varphi_1(\tau)\cdot u^n_i(x) + \varphi_2(\tau)\cdot u^{n-1}_i(x) \tag{6}$$

$$\dot{u}_i(x,\tau) = \dot{\varphi}_1(\tau)\cdot u^n_i(x) + \dot{\varphi}_2(\tau)\cdot u^{n-1}_i(x) \tag{7}$$

$$p_i(x,\tau) = \varphi_1(\tau)\cdot p^n_i(x) + \varphi_2(\tau)\cdot p^{n-1}_i(x) \tag{8}$$

Where $\varphi_1(\tau)$ and $\varphi_2(\tau)$ are linear temporal shape functions, which are expressed by Eq. (9):

$$\varphi_1(\tau) = \frac{\tau - T_{n-1}}{\Delta t} \quad \& \quad \varphi_2(\tau) = \frac{T_n - \tau}{\Delta t} \quad \& \quad T_{n-1} \prec \tau \prec T_n \tag{9}$$

Subscripts 1 and 2 mention to the forward and backward temporal nodes, during a time step, respectively. Therefore, the time integration including only the kernels and is represented by Eqs. (10), (11), (12), and (13):

https://doi.org/10.1016/j.heliyon.2018.e01114
2405-8440/© 2018 Published by Elsevier Ltd. This is an open access article under the CC BY-NC-ND license (http://creativecommons.org/licenses/by-nc-nd/4.0/).

$$G_{ij1}^{N-n+1} = (1-\eta)^{(N-n+1)\Delta t/2T} \int_{(n-1)\Delta t}^{n\Delta t} G_{ij}(x,s,t-\tau)\ \varphi_1(\tau)\cdot d\tau \tag{10}$$

$$G_{ij2}^{N-n+1} = (1-\eta)^{(N-n+1)\Delta t/2T} \int_{(n-1)\Delta t}^{n\Delta t} G_{ij}(x,s,t-\tau)\varphi_2(\tau)d\tau \tag{11}$$

$$F_{ij1}^{N-n+1} = (1-\eta)^{(N-n+1)\Delta t/2T} \int_{(n-1)\Delta t}^{n\Delta t} \left(Z_{ij}(x,s,t-\tau)\varphi_1(\tau) - W_{ij}(x,s,t-\tau)\dot{\varphi}_1(\tau)\right)d\tau \tag{12}$$

$$F_{ij2}^{N-n+1} = (1-\eta)^{(N-n+1)\Delta t/2T} \int_{(n-1)\Delta t}^{n\Delta t} \left(Z_{ij}(x,s,t-\tau)\varphi_2(\tau) - W_{ij}(x,s,t-\tau)\dot{\varphi}_2(\tau)\right)d\tau \tag{13}$$

After spatial discretization and some rebuilding, the complicated boundary element method equation for linear temporal variation can be expressed as Eq. (14):

$$c_{ij}\cdot u_i^N(s) = \sum_{n=1}^{N}\sum_{q=1}^{Q}\left\{T_{ik}^n \int_{\Gamma_q}\left[G_{ij}^{N+1-n}(r)\right]\cdot\overline{N}_k(\eta)\cdot|J|\cdot d\eta - U_{ik}^n\cdot\int_{\Gamma_q}\left[F_{ij}^{N+1-n}(r)\right]\cdot\overline{N}_k(\eta)\cdot|J|\cdot d\eta\right\} + u_{jd}^{inc.}(s,t) \tag{14}$$

The following description can be called linear time-convoluted visco-elastodynamic displacement and traction kernels, subsequently through Eqs. (15) and (16):

$$G_{ij}^{N-n+1}(r) = \left[G_{ij1}^{N-n+1}(r) + G_{ij2}^{N-n}(r)\right](1-\eta)^{(N-n+1)\Delta t/2T} \tag{15}$$

$$F_{ij}^{N-n+1}(r) = \left[F_{ij1}^{N-n+1}(r) + F_{ij2}^{N-n}(r)\right](1-\eta)^{(N-n+1)\Delta t/2T} \tag{16}$$

In the above equations, N and Q can show the last time step and the total number of boundary elements, respectively and L demonstrates the incorporation function of an isoperimetric quadratic boundary element. The two-dimensional full space visco-elastodynamic kernels, which have been derived analytically [27].

By sequentially writing Eq. (14) for each boundary node at time t+Δt, and with some rearrangement, the assembled system of equation takes the following matrix form in Eqs. (17) and (18):

https://doi.org/10.1016/j.heliyon.2018.e01114
2405-8440/© 2018 Published by Elsevier Ltd. This is an open access article under the CC BY-NC-ND license (http://creativecommons.org/licenses/by-nc-nd/4.0/).

$$F^{\mathbf{1}} \cdot U^{\mathbf{N}} = G^{\mathbf{1}} \cdot T^{\mathbf{N}} + Z^{N} \tag{17}$$

In which:

$$Z^{N} = \sum_{n=1}^{N-1} \left(G^{N-n+1} \cdot T^{n} - F^{N-n+1} \cdot U^{n} \right) + U_{d}^{inc.N} \tag{18}$$

In the above equations, U^N and T^N demonstrate the nodal movement and traction vectors at the current time node, subsequently. Z^N involves both the effects of the past dynamic history and the incident waves on the current time node [29, 30, 31, 32].

2.3. Model

The presented viscoelastic boundary element algorithm and derived time convoluted kernels are applied in a program code, which is named "VBEMSA" (Viscoelastic BEM for seismic analyses) to conduct investigation of topographic structures exposed to incoming waves including SV and P. Fig. 1 represents the shape and discretization of a semi-circular canyon exposed to vertically propagating incoming waves including SV and P by Eq. (19):

$$f(t) = A_{\max} \left[1 - 2\left(\pi f_p (t - t_0) \right)^2 \right] e^{-\left(\pi f_p (t - t_0) \right)^2} \tag{19}$$

In which, f_p and t_0 demonstrate the dominant frequency and a proper time shift factor, subsequently. $f(t)$ determines the horizontal part of the incoming displacement whenever the vertical one is equal to zero for SV, and it would be vice versa for P waves. Fig. 2 illustrates a layer, which is soft wit following parameters: height = 10 m, S_V = 70.5 m/s, overlying a stiffer half-space with $S_{V=}$141 m/s.

Different material damping ratios of 0.03, 0.06 and 0.10 is considered for soft layer. The amounts of 2.0 ton/m^3 and 0.33 are selected for densities and the Poisson's ratios, subsequently.

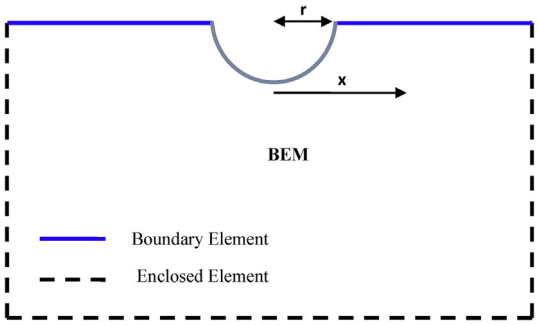

Fig. 1. Schematic geometry and discretization of a semi-circular canyon subjected to vertically propagating incident SV and P waves of the Ricker type.

https://doi.org/10.1016/j.heliyon.2018.e01114
2405-8440/© 2018 Published by Elsevier Ltd. This is an open access article under the CC BY-NC-ND license (http://creativecommons.org/licenses/by-nc-nd/4.0/).

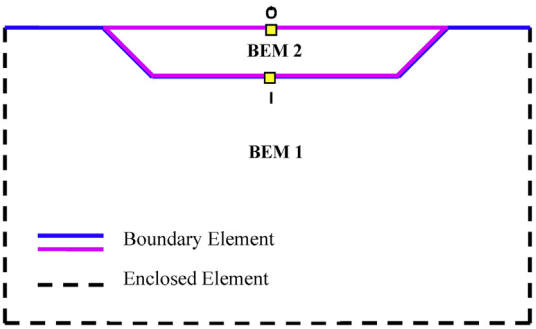

Fig. 2. Geometry and discretization of the layered half-plane problem.

The same examples are also analyzed with the SHAKE program, which is employed for 1-D analysis of site response [33]. A comparison of the horizontal acceleration time histories calculated by mentioned programs (SHAKE and VBEMSA)for the top (O) and bottom (I) of the soft layer can be seen in Figs. 3 and 4, subsequently. It may be observed that there is a good compatibility between the acquired results.

A semi-elliptical hill, as represented in Fig. 5, is exposed to the vertically propagating Ricker type P wave. This issue was investigated in a dimensionless form by Alvarez-Rubio et al. [34] for viscoelastic media. The Ricker wave has a predominant frequency of 2 Hz, time shift parameter of 0.8 s and maximum amplitude of 0.001 m. The hill has a radius of 200 m and height of 400m. The shear wave velocity, damping ratio, Poisson's ratio and mass density are 800 m/s, 0.25, 1% and 2.23 ton/m^3, subsequently.

Fig. 6 shows the amplifications acquired by the offered VBEMSA program along the canyon with those acquired by the previous study for a frequency of 1.5 ($\Omega = 1.5$).

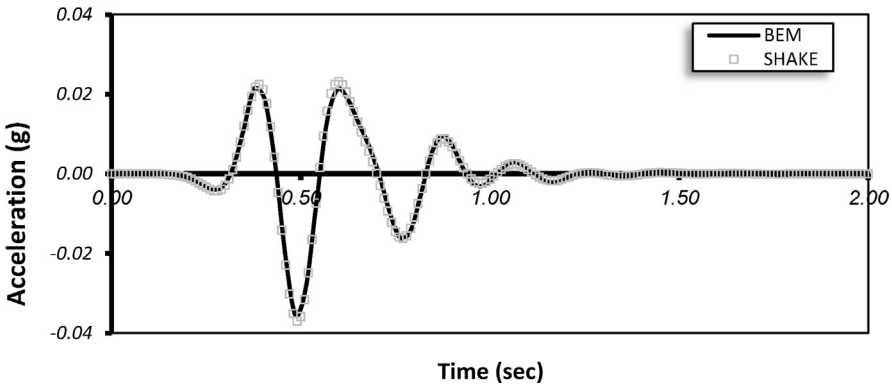

Fig. 3. Horizontal acceleration time histories at the base of the viscoelastic soft layer (point I) for material damping ratio 0.06.

https://doi.org/10.1016/j.heliyon.2018.e01114
2405-8440/© 2018 Published by Elsevier Ltd. This is an open access article under the CC BY-NC-ND license (http://creativecommons.org/licenses/by-nc-nd/4.0/).

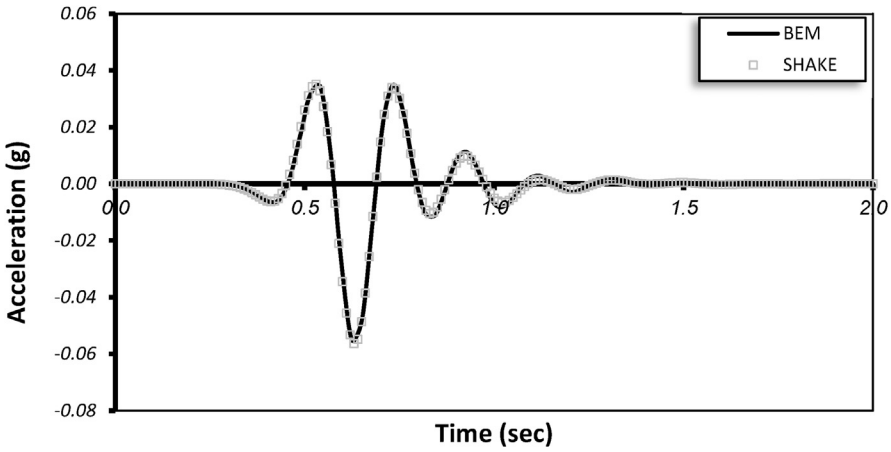

Fig. 4. Horizontal acceleration time histories at the top of the viscoelastic soft layer (point O) for material damping ratio 0.06.

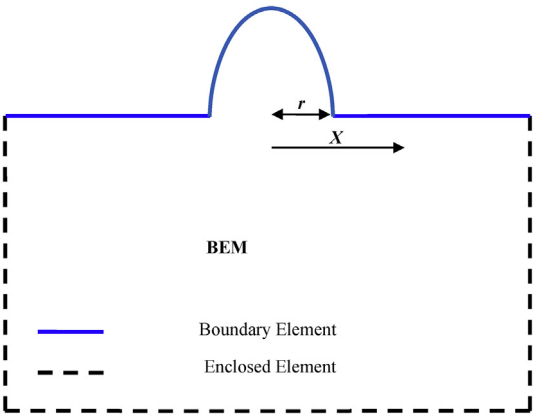

Fig. 5. Schematic geometry and discretization of a semi-elliptical hill subjected to vertically propagating incident SV and P waves of the Ricker type.

3. Results & discussion

In this research, we investigate the behavior of single hills and adjacent double and triple homogenous hills with shape ratios 0.1, 0.3, 0.5 and 0.7 with damping materials, 0.00, 0.03 and 0.06 under the effect of P and SV waves with the modeled dimension ranges from ± 5000 to ± 7240 m for semi-sine hills. The geometric characteristics of adjacent double semi-sine hills are provided in Fig. 7. The reason for choosing this amounts is that they are most used in previous studies in addition, the extensive studies to ensure hills behavior with different specifications seems sufficient.

https://doi.org/10.1016/j.heliyon.2018.e01114
2405-8440/© 2018 Published by Elsevier Ltd. This is an open access article under the CC BY-NC-ND license (http://creativecommons.org/licenses/by-nc-nd/4.0/).

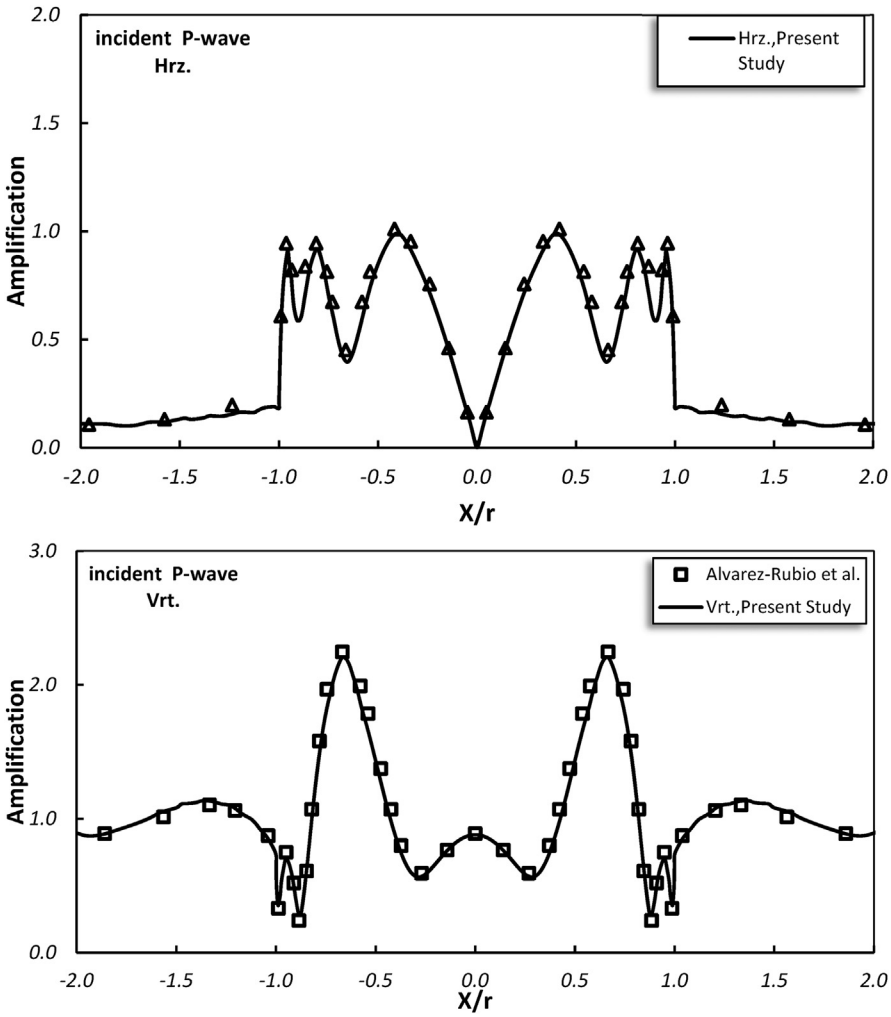

Fig. 6. Amplification of surface displacements for a semi-elliptical hill in the case of an incident P wave and $\Omega = 1.5$. (The symbols "Hrz" and "Vrt" represent the horizontal and vertical components of amplification, respectively.)

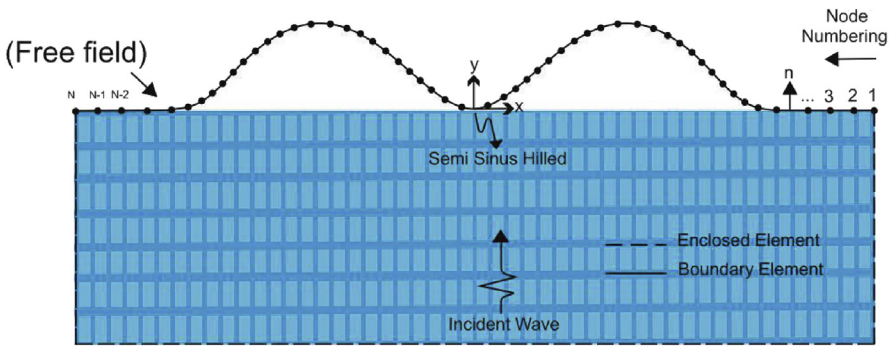

Fig. 7. Geometric properties of homogeneous adjacent double semi-sine hills.

https://doi.org/10.1016/j.heliyon.2018.e01114
2405-8440/© 2018 Published by Elsevier Ltd. This is an open access article under the CC BY-NC-ND license (http://creativecommons.org/licenses/by-nc-nd/4.0/).

3.1. Displacement pattern (time-place-displacement) for the hill

Fig. 8 shows graphs of vertical displacement component of ranges around double adjacent semi-sine hill for P and SV waves, Poisson's ratio 0.33, shape ratio 0.5 and all damping ratios including 0, 0.03 and 0.06 which are represented in Fig. 8a, b and c, respectively.

Observations from Fig. 8 can be stated that in the semi-sine hills, each point on the topography surface can create wave propagation. Wave propagation begins from the first moments of the incident wave hit to topography from two points in domain. By increasing distance from the hill, the propagated waves from different parts of the topography will interact and create a wave train per each phase. Increasing the ratio of hill shape can lead to rising the domain ranges of propagated waves; as a result, the motion time of points will be increased. The displacement pattern in the range of hills due to the adjacent hills has many complexities. In addition, to the propagated waves inside each of the hills, other propagated waves influence on the displacement pattern because of the surrounding hills.

Careful consideration of Fig. 8 (a), (b) and (c) represents that increasing damping can lead to reducing displacement along the hill and the motion time of points will be decreased. In addition, the range of error waves that are emitted is smaller and this issue can create a condition for surveying results in a greater range. Increased number of hills increases the complexity of displacement pattern and increases motion time of points.

Time history of vertical displacement of hill's crest, adjacent point of the reference hill with different shape ratio and affected by P waves in triple hills are presented in Figs. 9 and 10. As it can be seen in the central hill's crest, we will have longer time and an increase in the peak and valley points by increasing the shape ratio. However, a similar behavior can be seen in the hills crest by drawing time history in different shape ratio.

As it can be observed, as damping increases, displacement along the hills decreases, as a result the motion time will be decreased. Also, amplitude of error waves that are emitted from trimming range are smaller and this issue can create a condition for surveying the results in a greater range of the surrounding. Increasing the number of hills adds the complexity of the displacement pattern and increases motion time. Time history of vertical displacement of triple hill's crest are presented in various shape proportions and under the effect of SV waves in Fig. 11.

3.2. Amplification pattern (frequency-place−amplification) for the hill

Fig. 12 depicts amplification pattern (frequency-place-amplification) for a single, double and triple adjacent semi-sine hill for damping ratios of 0.0, 0.03 and 0.06

https://doi.org/10.1016/j.heliyon.2018.e01114
2405-8440/© 2018 Published by Elsevier Ltd. This is an open access article under the CC BY-NC-ND license (http://creativecommons.org/licenses/by-nc-nd/4.0/).

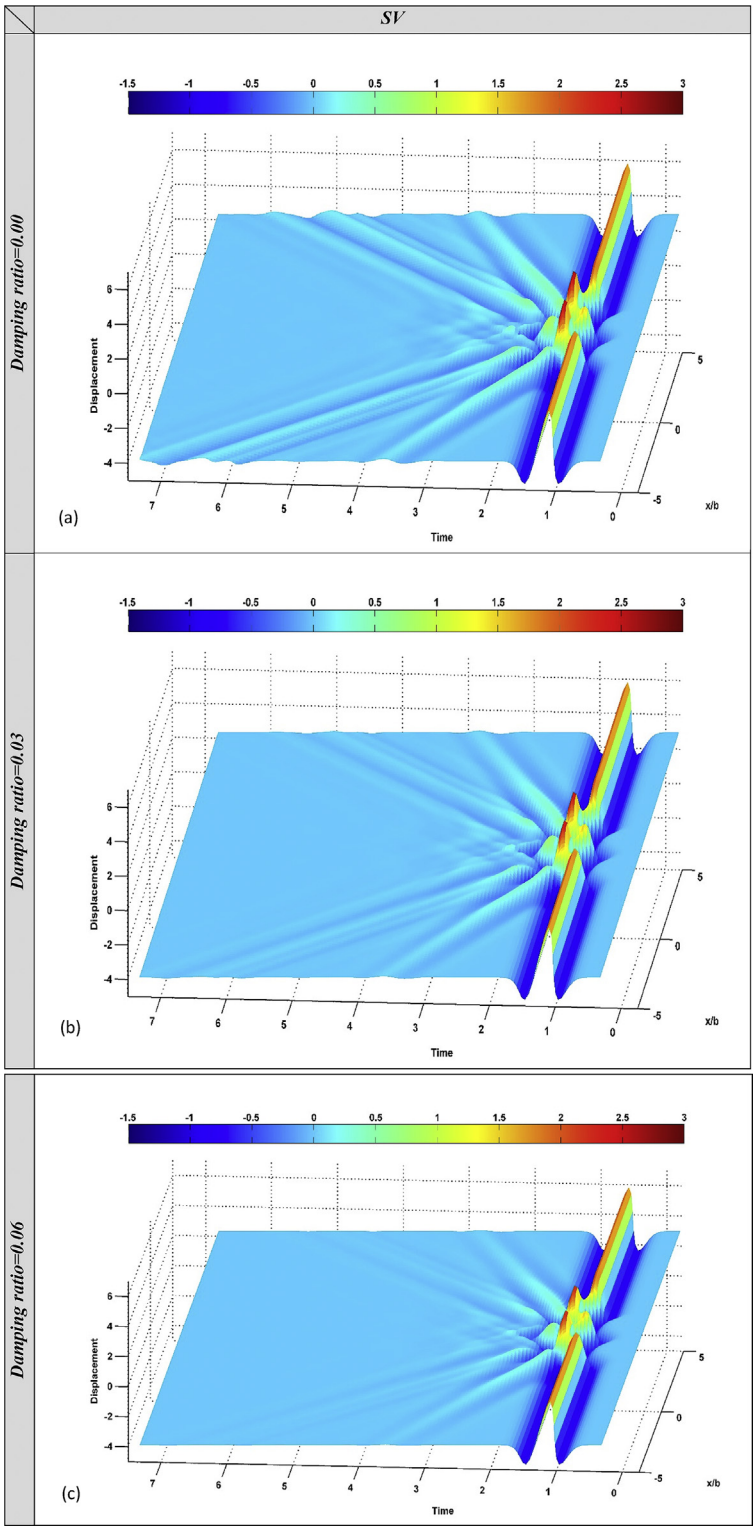

Fig. 8. Vertical and horizontal displacement pattern of double adjacent semi-sine hills for Poisson's ratio 0.33 and for shape ratio 0.5 and different damping factors in the vertical incident SV waves, (a) Damping ratio: 0.0, (b): Damping ratio: 0.03 and (c) Damping ratio: 0.06, respectively.

https://doi.org/10.1016/j.heliyon.2018.e01114
2405-8440/© 2018 Published by Elsevier Ltd. This is an open access article under the CC BY-NC-ND license (http://creativecommons.org/licenses/by-nc-nd/4.0/).

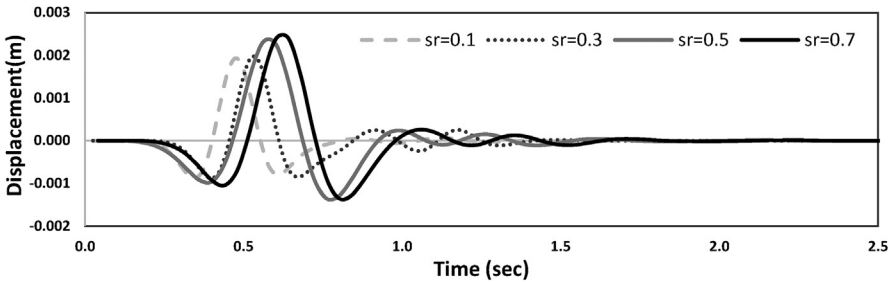

Fig. 9. Comparing the time history curves in central hill's crest in triple homogeneous hills in different shape ratios with damping ratio 3%.

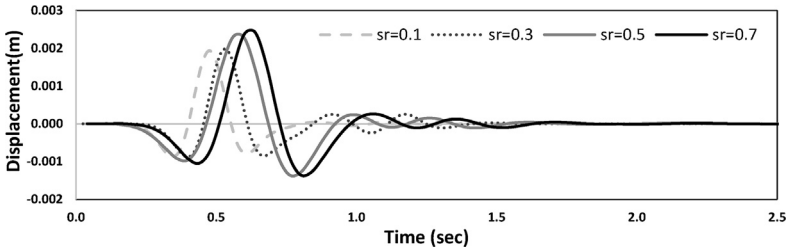

Fig. 10. Comparing the time history curves of the central hill's crest in triple homogeneous hills in different shape ratios with damping ratio 6%.

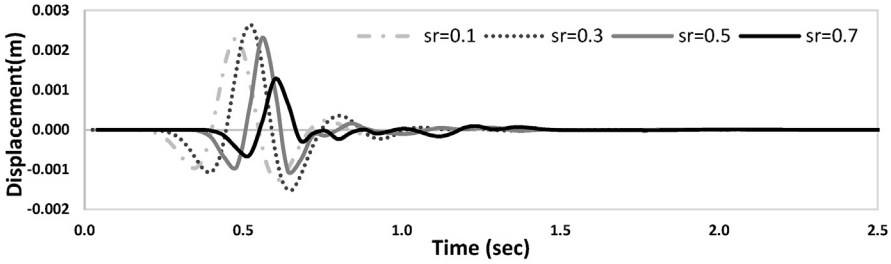

Fig. 11. Comparing the time history curves in the central hill's crest in triple homogeneous hills in different shape ratios with damping ratio 6%.

in Fig. 12 (a), (b) and (c). The trend of amplification function is slow and gradual due to the homogeneous geometry of semi-sine hill. Increasing the hill shape ratio can lead to growing the effect of seismic response. Surveying the behavior of the points on the hill indicates that by increasing incident wave period in comparison with characterized period of the topography; their motion will be uniform and closer to the free field movement. Increasing the distance of the points from the hill's center can lead to increasing the amplification and de-amplification sequence. Results of Fig. 12 (a), (b) and (c) shows that by increasing the material-damping ratio, the amplification potential is reduced on hill's crest and such effect is considerable in the site specified period. Moreover, the effect of material damping ratio on amplification potential is more tangible with increasing hill's shape ratio.

https://doi.org/10.1016/j.heliyon.2018.e01114
2405-8440/© 2018 Published by Elsevier Ltd. This is an open access article under the CC BY-NC-ND license (http://creativecommons.org/licenses/by-nc-nd/4.0/).

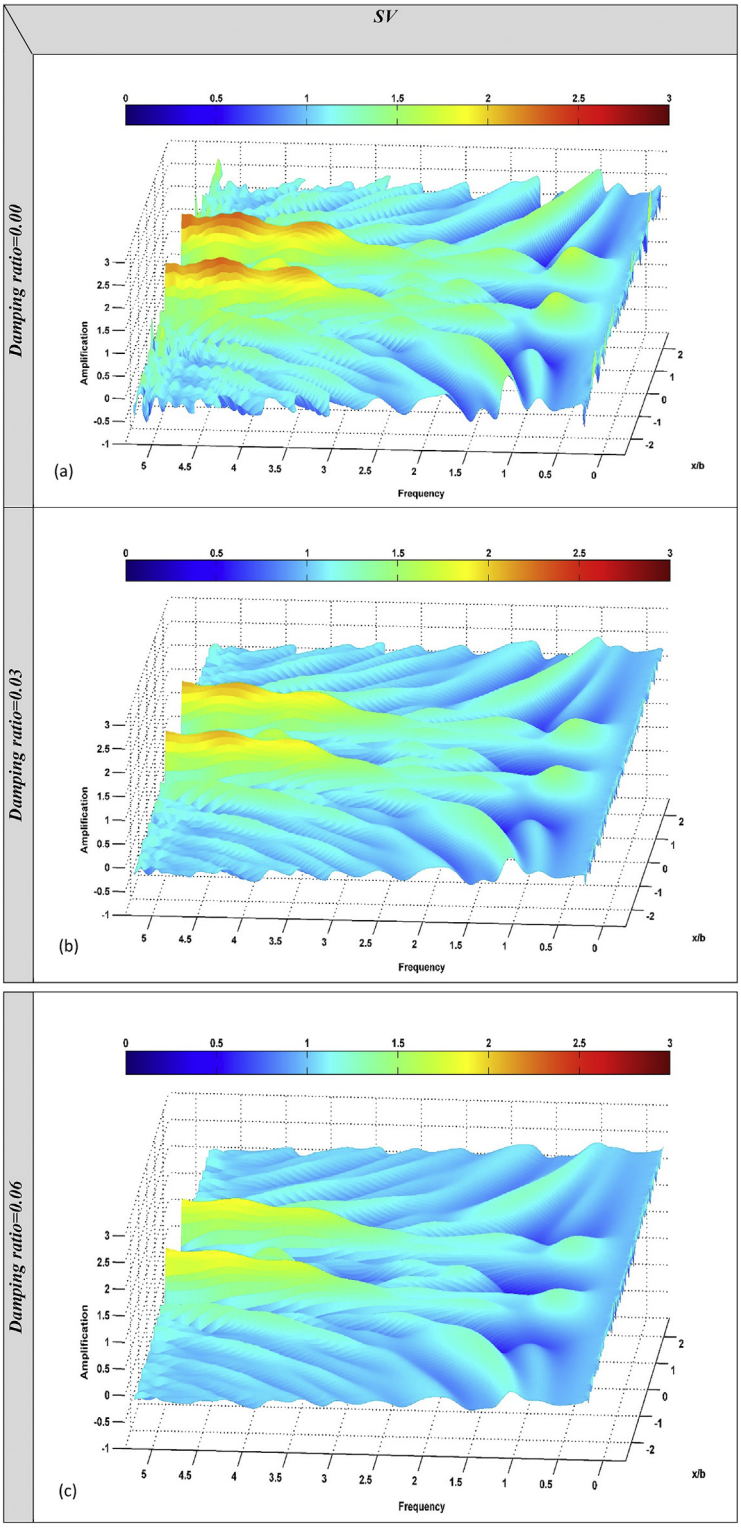

Fig. 12. Vertical and horizontal component of amplification of double adjacent semi-sine hills for shape ratio (0.5) and different damping factors for incident SV wave, (a) Damping ratio: 0.0, (b): Damping ratio: 0.03 and (c) Damping ratio: 0.06, respectively.

https://doi.org/10.1016/j.heliyon.2018.e01114
2405-8440/© 2018 Published by Elsevier Ltd. This is an open access article under the CC BY-NC-ND license (http://creativecommons.org/licenses/by-nc-nd/4.0/).

3.3. Amplification curves on hill's crest

Crest point behavior in the single, double and triple homogeneous adjacent hills is represented in Fig. 13. In this Fig, the amplification curves at the hill's crest are compared for different shape ratios and damping. Examination of these curves shows that:

Crest of double adjacent hills in comparison with single hills has similar shape ratio, and greater potential and amplification maximization. Although this difference increases with increasing shape ratio, it is negligible within the studied shape ratio. However, by increasing the number of hills, the growth has an ascending trend and we even

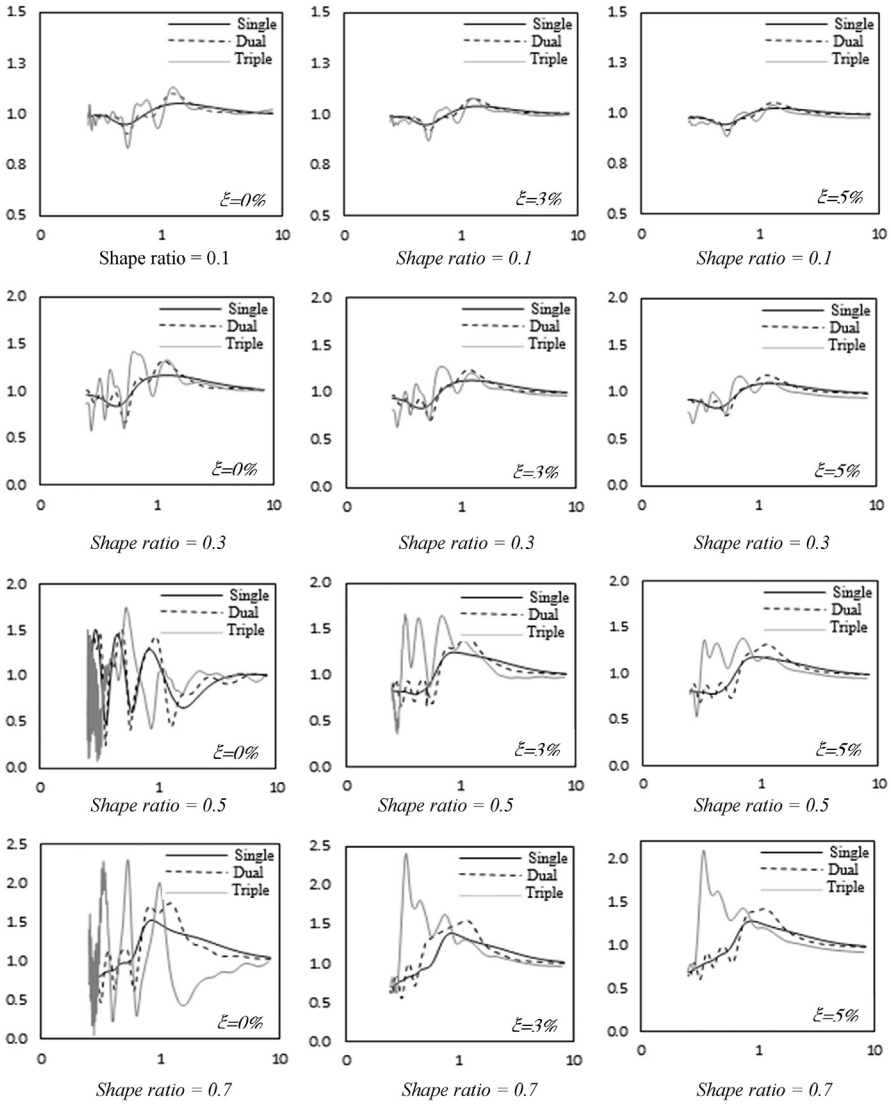

Fig. 13. Compares crest amplification curve for single, double and triple adjacent hills in the shape ratio and different damping factors - the vertical axis is amplification and the horizontal axis is the dimensionless period.

https://doi.org/10.1016/j.heliyon.2018.e01114
2405-8440/© 2018 Published by Elsevier Ltd. This is an open access article under the CC BY-NC-ND license (http://creativecommons.org/licenses/by-nc-nd/4.0/).

observe different behavior in higher shape ratio. In addition, by increasing the damping ratio of material, the difference between the top and bottom points will be reduced.

- Behavior of single and double adjacent hills is somewhat similar to each other but by increasing the shape ratio in triple adjacent hills, we have a different behavior. Although, by increasing the shape ratio, a different behavior in triple adjacent hills than the other two modes can be observed, this difference occurs in short periods and it is equal in long periods. The value of this similarity is more tangible by increasing damping ratio. Moreover, in shorter periods, number of hills, frequency characteristics of the amplification curves and the number of peaks and valleys is increased.
- The similarity in long periods is because the crest response in both adjacent and single hills tends to seismic response of free field. However, this similarity cannot be seen in short periods. Most changes at the amplification curves is observed in the crest of semi-sine double hills in both states of placement at intermediate periods. Increasing number of hills and examining the amplification curves in hill's crest shows that by increasing number of hills, maximum amplification occurs earlier and at lower periods, so that the maximum occurred very quickly in triple hills in high shape ratios.
- By increasing damping ratio, although complication period has no significant change, but it reduces the amplification potential in the hill's crest and the effect is more in the specified period and has significantly reduced the amplification potential. The effect of amplification amounts is more tangible than the damping ratio of materials by increasing the hill shape ration.

3.4. Amplification of edge and central points at semi-sine hills with damping ratio

Fig. 14 illustrates the single, double and triple adjacent semi-sine hills in Fig. 14 (A), (B) and (C), respectively. Fig. 15 compares the amplification of edges of single,

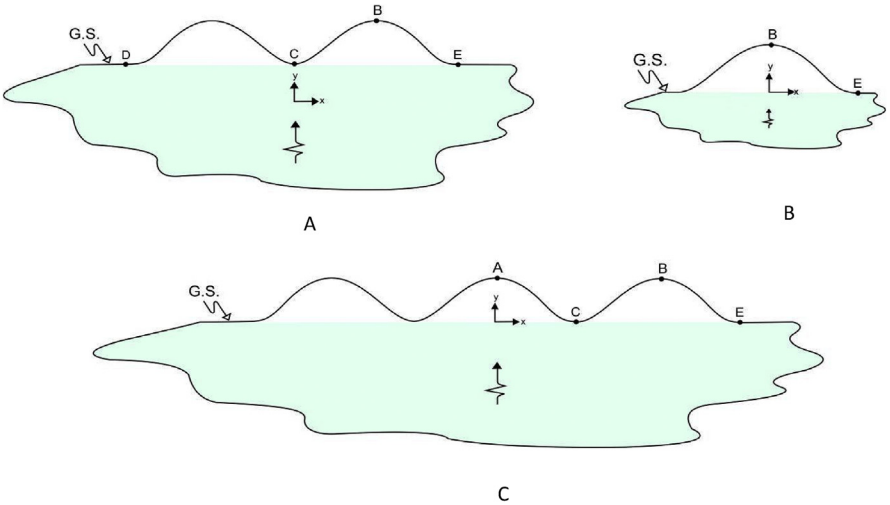

Fig. 14. Homogenous semi-sine hills (A): Single, (B): Double and (C): Triple.

https://doi.org/10.1016/j.heliyon.2018.e01114
2405-8440/© 2018 Published by Elsevier Ltd. This is an open access article under the CC BY-NC-ND license (http://creativecommons.org/licenses/by-nc-nd/4.0/).

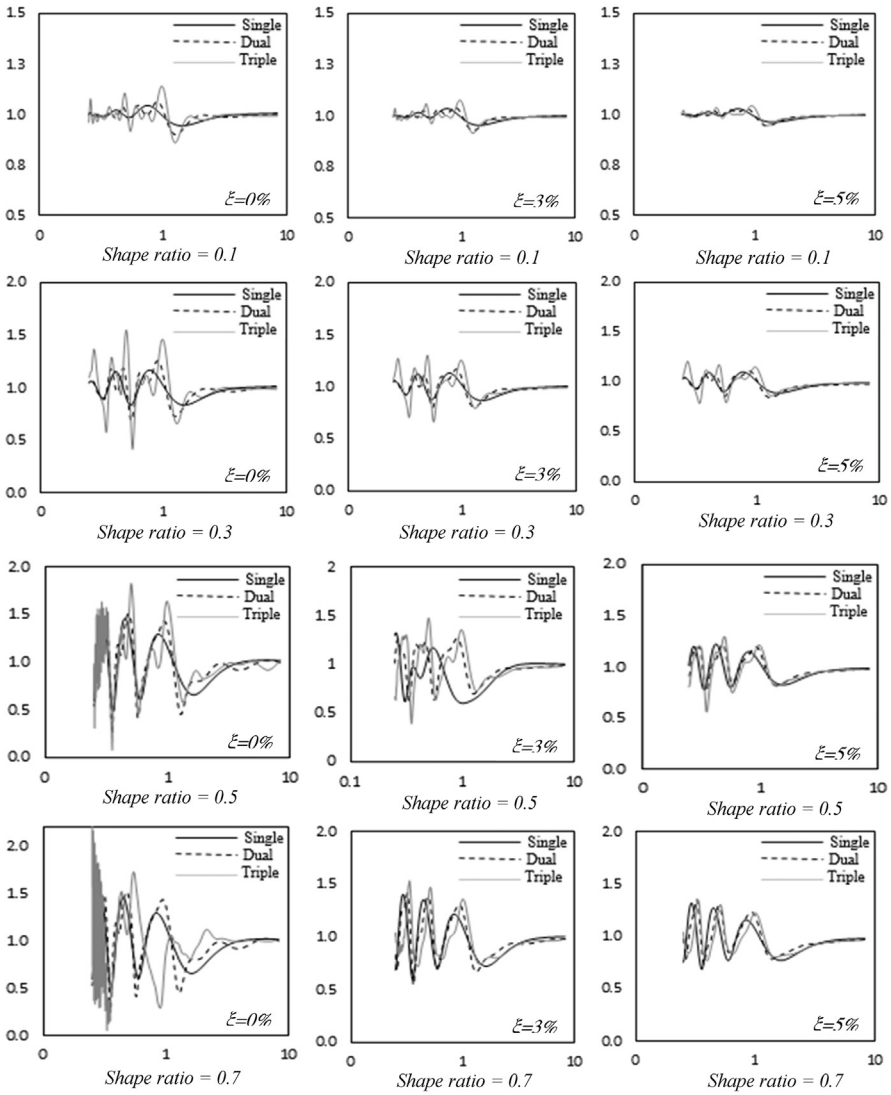

Fig. 15. Shows the comparison of amplification curve of the hill edge (point E) for single, double and triple adjacent homogenous hills in shape ration and different damping factor of dimensionless horizontal axis and vertical axis of corresponding amplification.

double and triple homogenous adjacent hills (point E of Fig. 14A, B and C), in different damping ratios. In addition, Fig. 16 compared amplification of the midpoint of the double and triple homogenous hills (point C of Fig. 14B and C) with different damping ratios. Examining amplification curves at these points show that:

Edge of adjacent hills compared with edges of single hills with similar shape ratio, has greater potential and larger microzonation maximum. The difference between amplification values of single and adjacent hills will be reduced by increasing material damping ratio. Increasing the maximum amplification by enhancing shape ratio has an increasing trend and direct relationship with each other. Moreover,

https://doi.org/10.1016/j.heliyon.2018.e01114
2405-8440/© 2018 Published by Elsevier Ltd. This is an open access article under the CC BY-NC-ND license (http://creativecommons.org/licenses/by-nc-nd/4.0/).

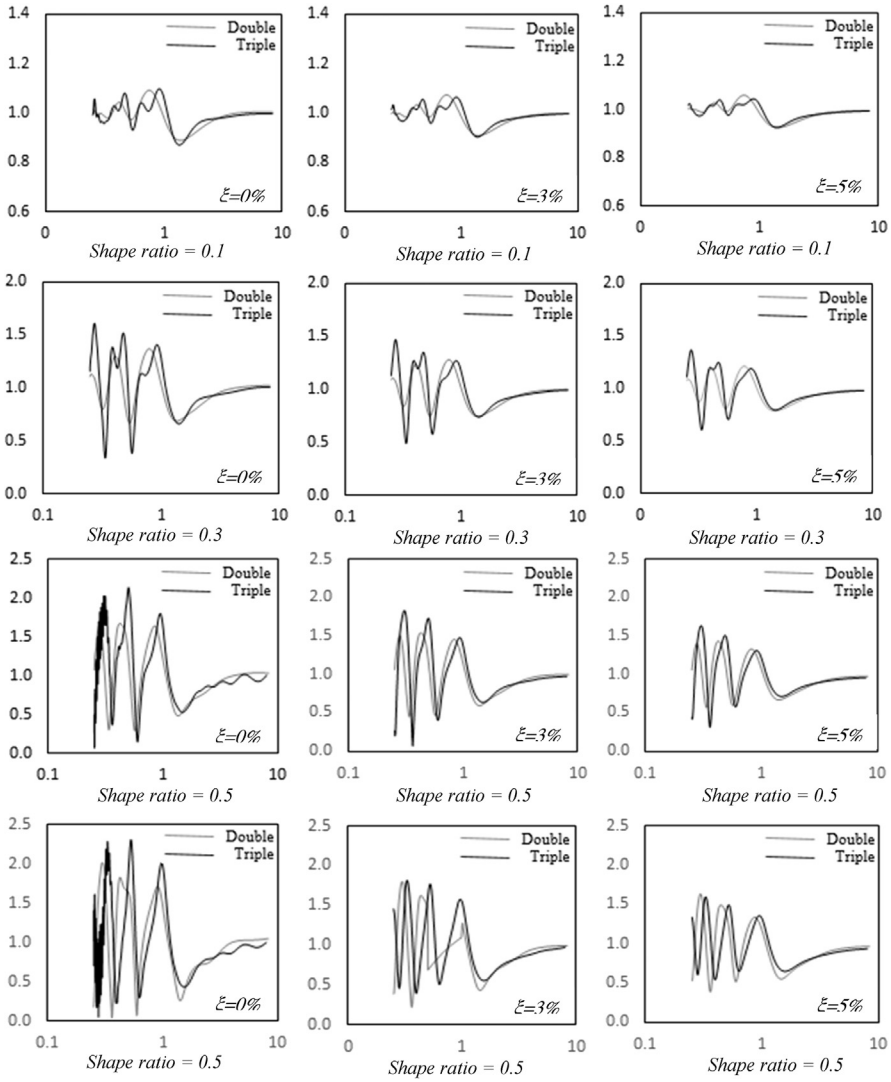

Fig. 16. Shows the comparison between amplification curve of midpoint (point C) for homogenous double and triple adjacent hills in shape ratio and different damping factors in dimensionless horizontal axis and vertical axis of corresponding amplification.

multiplicity of hills can lead to increasing the frequency characteristics of the amplification curve and the number of peaks and valleys.

The external edge of double hills has a seismic behavior similar to single hills at the incident of long and short waves.

Maximum amplification at edge of double hills occurs in longer periods compared with single hills, but in triple hills, maximum amplification occurs at shorter intervals even in comparison the single hills. A relatively similar behavior is observed in the edge of adjacent or single hills such as long periods but the similarity cannot be seen in shorter

https://doi.org/10.1016/j.heliyon.2018.e01114
2405-8440/© 2018 Published by Elsevier Ltd. This is an open access article under the CC BY-NC-ND license (http://creativecommons.org/licenses/by-nc-nd/4.0/).

periods, and even a dramatic difference can be seen in triple hills. In addition, by increasing the damping ratio, adjacent and single hills' behavior will be very similar.

The points between triple homogenous hills compared with double homogenous hills have similar shape ratio, and greater potential and maximum amplification and microzonation. Points among the triple homogenous hills compared to double homogenous hills have more peaks and this peak will be highlighted by increasing the shape ratio. In addition, the adjacent hills will have similar behavior to each other by increasing the damping ratio of the midpoints.

The maximum amplification in the points between triple homogenous hills will occur at shorter periods than the double hills (like Point E). By increasing material damping ratio, the difference between amplification of adjacent double and triple hills in points among hills will be less (like Point E).

4. Conclusion

The study represents an overview of amplification model of 2D homogenous semi-sine shaped hills with material damping exposed to vertical incoming waves including SV and P, acquired by numerical analyses using the time domain BEM. The main conclusions of the analysis are as follows:

1- Looking at the trends of amplification function changes along the topography, a slow and gradual process is observed and the effect of its seismic response will be increased by increasing the hill shape ratio according to the geometry of homogenous semi-sine hill.

2- As it can be seen in the displacement patterns, the motion time of the points and displacement along the hill will be reduced by increasing damping.

3- Material damping changes does not affect the hill amplification pattern, but potential amplification in and out will be decreased by increasing damping ratio.

4- At the time of completion of the analysis in triple adjacent hills without damping of materials with high shape ratio, there is still amplification in and out, while this cannot be observed in similar analyzes with damping materials. This issue can show the effect of wave interference and criticality of this effect in the adjacent hills.

5- Triple hill's crest compared with double hill's crest with the same shape proportion, has the greater amplification potential, which this difference is reduced by increasing damping materials.

6- In amplification curves, in the double homogenous semi-sine hill's crest in the long periods, a relatively similar behavior can be seen in the crest of double homogenous adjacent hills and single hills. The value of this similarity is

https://doi.org/10.1016/j.heliyon.2018.e01114
2405-8440/© 2018 Published by Elsevier Ltd. This is an open access article under the CC BY-NC-ND license (http://creativecommons.org/licenses/by-nc-nd/4.0/).

more tangible by increasing material damping, but there are no such similarities in short periods.

7- Most changes in amplification curves are observed in the semi-sine hill's crest in intermediate periods.

8- Edges of the adjacent hills compared with the edges of single hills have similar shape ratio and greater potential.

9- Growth of maximum amplification ratio has an upward trend by increasing the number of hills and shape ratio and has a direct relationship with them.

10- Frequency specifications of amplification curve and the number of peaks and valleys will be increased by increasing the number of hills.

11- The maximum amplification in points between triple homogenous hills compared with double homogenous hills occurs in shorter periods (e.g., point E).

12- Hills with any shape ratio, regardless of damping, have special response spectrum.

13- The number of hills has no effect on the response spectrum in a particular shape proportion and the influence of the number of hills in drawing the response spectrum can be ignored.

14- Material damping like amplification and displacement affects the response spectrum.

Declarations

Author contribution statement

Mobin Afzalirad, Mehran Naghizadehrokni, Iman Khosravi: Conceived and designed the analysis; Analyzed and interpreted the data; Wrote the paper.

Funding statement

This research did not receive any specific grant from funding agencies in the public, commercial, or not-for-profit sectors.

Competing interest statement

The authors declare no conflict of interest.

Additional information

No additional information is available for this paper.

https://doi.org/10.1016/j.heliyon.2018.e01114
2405-8440/© 2018 Published by Elsevier Ltd. This is an open access article under the CC BY-NC-ND license (http://creativecommons.org/licenses/by-nc-nd/4.0/).

References

[1] P.Y. Bard, P. Gueguen, J.L. Chazelas, M. Kham, J.F. Semblat, Seismic hazard in urban environments: can man modify the hazard?, in: Proc. of 3ed Congreso Nacional de Ingeniería Sísmica, Juan-Bautista Martínez-Guevara CIMNE, Barcelona, 2007.

[2] M.A. Sandıkkaya, S. Akkar, P.Y. Bard, E. Engineering, A Probabilistic Procedure to Describe Site Amplification Factors for Seismic Design Codes, Soil Dynam. Earthq. Eng. (2018).

[3] Z. Ba, X. Yin, Wave scattering of complex local site in a layered half-space by using a multidomain IBEM: incident plane SH waves, Geophys. J. Int. 205 (3) (2016) 1382−1405.

[4] M.K. Bakavoli, E. Haghshenas, J.B. Bazzaz, M. Bakavoli, Effect of nearby topography on amplification of seismic motion in topographic irregularities: the case of a hilly side in Tehran, in: 15th World Conference on Earthquake Engineering, Lisboa, Portugal, 2012.

[5] M.D. Trifunac, D.E. Hudson, Analysis of the Pacoima dam accelerogram—San Fernando, California, earthquake of 1971, Bull. Seismol. Soc. Am. 61 (5) (1971) 1393−1411.

[6] D.M. Boore, The effect of simple topography on seismic waves: implications for the accelerations recorded at Pacoima Dam, San Fernando Valley, California, Bull. Seismol. Soc. Am. 63 (5) (1973) 1603−1609.

[7] M.D. Trifunac, Site conditions and earthquake ground motion−A review, Soil Dynam. Earthq. Eng. 90 (2016) 88−100.

[8] D.M. Boore, What do data used to develop Ground-Motion Prediction Equations tell us about motions near faults? Pure Appl. Geophys. 171 (11) (2014) 3023−3043.

[9] W. Lee, R. White, D. Harlow, J. Rogers, P. Spudich, D. Dodge, Digital Seismograms of Selected Aftershocks of the Northridge Earthquake Recorded by a Dense Seismic Array on February 11, 1994 at Cedar Hill Nursery in Tarzana, California, US Geological Survey 2331-1258, 1994.

[10] A. Amornwongpaibun, H. Luo, V.W. Lee, Scattering of anti-plane (SH) waves by a shallow semi-elliptical hill with a concentric elliptical tunnel, J. Earthq. Eng. 20 (3) (2016) 363−382.

[11] M. Celebi, Topographical and geological amplifications determined from strong-motion and aftershock records of the 3 March 1985 Chile earthquake, Bull. Seismol. Soc. Am. 77 (4) (1987) 1147−1167.

https://doi.org/10.1016/j.heliyon.2018.e01114
2405-8440/© 2018 Published by Elsevier Ltd. This is an open access article under the CC BY-NC-ND license (http://creativecommons.org/licenses/by-nc-nd/4.0/).

[12] L.L. Davis, L.R. West, Observed effects of topography on ground motion, Bull. Seismol. Soc. Am. 63 (1) (1973) 283−298.

[13] P. Bard, Discussion session: lessons, issues, needs and prospects, special theme session 5: Turkey Flat and Ashigara Valley experiments, in: Proc, 1992, pp. 6985−6988.

[14] M. Kamalian, M. Jafari, A. Sohrabi-Bidar, Seismic behavior of 2D semi-sine shaped hills against vertically propagating incident waves, Esteghlal J. Eng. 26 (1) (2007) 109−130.

[15] M. Kamalian, M.K. Jafari, A. Sohrabi-bidar, A. Razmkhah, B. Gatmiri, Time-domain two-dimensional site response analysis of non-homogeneous topographic structures by a hybrid BE/FE method, Soil Dynam. Earthq. Eng. 26 (8) (2006) 753−765.

[16] M. Kamalian, A. Sohrabi-Bidar, A. Razmkhah, A. Taghavi, I. Rahmani, Considerations on seismic microzonation in areas with two-dimensional hills, J. Earth Syst. Sci. 117 (2) (2008) 783−796.

[17] H. Alielahi, M. Kamalian, M. Adampira, A BEM investigation on the influence of underground cavities on the seismic response of canyons, Acta Geotech. 11 (2) (2016) 391−413.

[18] M. Kamalian, B. Gatmiri, A. Sohrabi-Bidar, A. Khalaj, Amplification pattern of 2D semi-sine-shaped valleys subjected to vertically propagating incident waves, Commun. Numer. Methods Eng. 23 (9) (2007) 871−887.

[19] M. Afzalirad, M. Kamalian, M. Jafari, A. Sohrabi-Bidar, Seismic behavior of topographic features with material damping using BEM in time domain, Int. J. Civ. Eng. Res. 12 (1 B) (2014) 26−44.

[20] M. Kamalian, M.K. Jafari, A. Sohrabi-Bidar, A. Razmkhah, Seismic response of 2-D semi-sine shaped hills to vertically propagating incident waves: amplification patterns and engineering applications, Earthq. Spectra 24 (2) (2008) 405−430.

[21] S. Chaillat, M. Bonnet, J.-F. Semblat, A new fast multi-domain BEM to model seismic wave propagation and amplification in 3-D geological structures, Geophys. J. Int. 177 (2) (2009) 509−531.

[22] A. Sohrabi-Bidar, M. Kamalian, M. Jafari, Time-domain BEM for three-dimensional site response analysis of topographic structures, Int. J. Numer. Methods Eng. 79 (12) (2009) 1467−1492.

https://doi.org/10.1016/j.heliyon.2018.e01114
2405-8440/© 2018 Published by Elsevier Ltd. This is an open access article under the CC BY-NC-ND license (http://creativecommons.org/licenses/by-nc-nd/4.0/).

[23] A. Sohrabi-Bidar, M. Kamalian, M.K. Jafari, Seismic response of 3-D Gaussian-shaped valleys to vertically propagating incident waves, Geophys. J. Int. 183 (3) (2010) 1429−1442.

[24] V. Di Fiore, Seismic site amplification induced by topographic irregularity: results of a numerical analysis on 2D synthetic models, Eng. Geol. 114 (3) (2010) 109−115.

[25] A. Cavallaro, A. Ferraro, S. Grasso, M. Maugeri, Topographic effects on the Monte Po hill in Catania (Italy), Soil Dynam. Earthq. Eng. 43 (2012) 97−113.

[26] P.W. Partridge, C.A. Brebbia, Dual Reciprocity Boundary Element Method, Springer Science & Business Media, 2012.

[27] J. Dominguez, Boundary Elements in Dynamics, Wit Press, 1993.

[28] F. Jin, O. Pekau, C.H. Zhang, A 2-D time-domain boundary element method with damping, Int. J. Numer. Methods Eng. 51 (6) (2001) 647−661.

[29] S. Ahmad, P.K. Banerjee, Multi-domain BEM for two-dimensional problems of elastodynamics, Int. J. Numer. Methods Eng. 26 (4) (1988) 891−911.

[30] A. Israil, P. Banerjee, Advanced time-domain formulation of BEM for two-dimensional transient elastodynamics, Int. J. Numer. Methods Eng. 29 (7) (1990) 1421−1440.

[31] A. Israil, P. Banerjee, Two-dimensional transient wave-propagation problems by time-domain BEM, Int. J. Solid Struct. 26 (8) (1990) 851−864.

[32] A. Israil, P. Banerjee, Advanced development of boundary element method for two-dimensional dynamic elasto-plasticity, Int. J. Solid Struct. 29 (11) (1992) 1433−1451.

[33] P.B. Schnabel, SHAKE a Computer Program for Earthquake Response Analysis of Horizontally Layered Sites, EERC Report, 1972, pp. 72-12.

[34] S. Alvarez-Rubio, F.J. Sánchez-Sesma, J.J. Benito, E. Alarcón, The direct boundary element method: 2D site effects assessment on laterally varying layered media (methodology), Soil Dynam. Earthq. Eng. 24 (2) (2004) 167−180.

https://doi.org/10.1016/j.heliyon.2018.e01114
2405-8440/© 2018 Published by Elsevier Ltd. This is an open access article under the CC BY-NC-ND license (http://creativecommons.org/licenses/by-nc-nd/4.0/).